GEOPHYSICS, VOL. 84, NO. 6 (NOVEMBER-DECEMBER 2019); P. EN81–EN92, 18 FIGS., 2 TABLES.
10.1190/GEO2018-0651.1





# Estimation of horizontal-to-vertical spectral ratios (ellipticity) of Rayleigh waves from multistation active-seismic records

Binbin Mi[1], Yue Hu[2], Jianghai Xia[1], and Laura Valentina Socco[3]

## ABSTRACT

The horizontal-to-vertical spectral-ratio (HVSR) analysis of ambient noise recordings is a popular reconnaissance tool used worldwide for seismic microzonation and earthquake site characterization. We have expanded this single-station passive HVSR technique to active multicomponent data. We focus on the calculation of the HVSR of Rayleigh waves from active-seismic records. We separate different modes of Rayleigh waves in seismic dispersion spectra and then estimate the HVSR for the fundamental mode. The mode separation is implemented in the frequency-phase velocity ($f$-$v$) domain through the high-resolution linear Radon transformation. The estimated Rayleigh-wave HVSR curve after mode separation is consistent with the theoretical HVSR curve, which is computed by solving the Rayleigh-wave eigenproblem in the laterally homogeneous layered medium. We find that the HVSR peak and trough frequencies are very sensitive to velocity contrast and interface depth and that HVSR curves contain information on lateral velocity variations. Using synthetic and field data, we determine the validity of estimating active Rayleigh-wave HVSR after mode separation. Our approach can be a viable and more accurate alternative to the empirical HVSR analysis method and brings a novel approach for the analysis of active multicomponent seismic data.

## INTRODUCTION

The horizontal-to-vertical spectral-ratio (HVSR) method is an analysis technique that calculates the ratio of the horizontal-to-vertical Fourier spectra derived from seismic noise or ambient vibration recordings, typically recorded at a specific location by a 3C broadband sensor. This single-station approach was introduced by Nakamura (1989). During the following quarter-century, this quick, reliable, and low-cost HVSR method has become an increasingly popular tool and is used worldwide for seismic site characterization to retrieve the resonance frequencies of unconsolidated sediments over the high-velocity bedrock (we refer the reader to the latest review paper by Molnar et al., 2018). However, the large use of HVSR analysis is predominantly a consequence of its ease in application rather than of a full understanding of its theory (Molnar et al., 2018). The recorded ambient noise is a mixture of various wave types (body and/or surface waves), which contain information on the sources and transmission paths of waves and subsurface structures (e.g., Lachet and Bard, 1994; Fäh et al., 2001; Okada, 2003; Malischewsky and Scherbaum, 2004). Recent developments in the theoretical basis of ambient noise HVSR response consider the noise wavefield as being comprised of diffuse waves (Sánchez-Sesma et al., 2011; Kawase et al., 2015; Lunedei and Albarello, 2015).

The physics behind the ambient noise HVSR manifestation is wavefield-dependent; i.e., it is composed of body, surface, or diffuse waves and/or combinations thereof (Molnar et al., 2018). It is, however, impossible to isolate every wave from a single-station noise record. Therefore, no single analytical expression exists as yet for all real-world conditions. An empirical equation for the HVSR peak frequencies in the model with a single soil layer over

Manuscript received by the Editor 4 October 2018; revised manuscript received 12 April 2019; published ahead of production 21 August 2019; published online 16 October 2019.
[1]Zhejiang University, School of Earth Sciences, 38 Zheda Road, Hangzhou 310027, China. E-mail: mibinbin1991@126.com; jianghai_xia@yahoo.com (corresponding author).
[2]Zhejiang University, School of Earth Sciences, 38 Zheda Road, Hangzhou 310027, China and Yangtze River Scientific Research Institute, Key Laboratory of Geotechnical Mechanics and Engineering of Ministry of Water Resources, Wuhan 430010, China. E-mail: huyue0716@foxmail.com.
[3]Politecnico di Torino, Department of Environment, Land and Infrastructure Engineering, 24 C.so Duca degli Abruzzi, Torino 10129, Italy. E-mail: valentina.socco@polito.it.

a stiff half-space is written as $f_n = n(V_{S1}/4h)$, where $V_{S1}$ and $h$ represent the S-wave velocity and thickness of the soil layer, respectively, and the index $n$ ($n = 1, 3, 5$, etc.) designates the $n$th mode of oscillation (Haskell, 1960). Bonnefoy-Claudet et al. (2008) demonstrate that this holds when noise records are composed of body and/or surface waves.

Regardless of the controversial theory, in many studies, the HVSR peak and/or its entire spectrum are inverted for the subsurface S-wave velocity $V_S$ structure (e.g., Fäh et al., 2003; Arai and Tokimatsu, 2004; Hobiger et al., 2013; Lontsi et al., 2015; Bignardi et al., 2016; García-Jerez et al., 2016; Piña-Flores et al., 2017), although the physics-based forward-modeling codes used in the inversion vary among different studies. Some researchers also jointly invert the HVSR and Rayleigh-wave dispersion curves for 1D S-wave velocity profiles (e.g., Picozzi et al., 2005; Gribler and Mikesell, 2016).

Our aim in this paper is to obtain the HVSR curve from active-seismic multicomponent records. We focus on Rayleigh waves, which are dominant in the P-SV wavefield. Rayleigh-wave data from active-seismic records can be used to estimate the near-surface S-wave velocity distribution by dispersion-curve inversion using the multichannel analysis of surface waves (MASW) method (Song et al., 1989; Miller et al., 1999; Park et al., 1999; Xia et al., 1999). During the past two decades, the MASW method has been efficiently applied to a wide range of problems in geotechnical and environmental engineering (Socco et al., 2010; Foti et al., 2011; Xia, 2014; Mi et al., 2017). Commonly, Rayleigh waves are obtained only from the vertical component of P-SV waves. However, the multimodal Rayleigh waves estimated from the horizontal (radial) component data have a different energy distribution compared with those estimated from the vertical component data (Dal Moro and Ferigo, 2011). The combined use of the horizontal component data with the vertical component data would contribute to preventing mode misidentification (Boaga et al., 2013) and improving S-wave velocity estimations (Ikeda et al., 2015).

The HVSR of Rayleigh waves is the ratio between the horizontal and vertical particle motions of Rayleigh waves, which is the ellipticity of Rayleigh waves. It strongly depends on the local soil structure over high-velocity bedrock (e.g., Fäh et al., 2001; Tuan et al., 2011; Hobiger et al., 2013). Boaga et al. (2013) illustrate that the Rayleigh-wave ellipticity polarization is linked to the mode osculation, which is the energy peak shifting from the fundamental to the first higher mode at low frequencies (e.g., Boaga et al., 2013; Mi et al., 2018). Large contrasts in the subsurface produce the mode osculation and a high peak (horizontal polarization) and a low trough (vertical polarization) in the ellipticity curve of the Rayleigh-wave fundamental mode (Boaga et al., 2013). Fäh et al. (2001) demonstrate in the ambient noise HVSR that the fundamental-mode Rayleigh wave is not the dominant wave type at the peak frequency; rather, higher mode Rayleigh waves are.

In active-seismic records, Rayleigh waves are dominant at more than one wavelength from the source, but the records also contain body and/or leaky waves (Gao et al., 2014) and/or noise. Moreover, the interference of different Rayleigh-wave modes may introduce errors in the calculation of HVSR for a specific mode. In this paper, we propose to separate different modes of Rayleigh waves from active seismic data and then estimate the HVSR using the part of the signal that is associated with the fundamental mode. After describing the methodology, we use a 1D synthetic model to show that it is necessary to separate different modes of Rayleigh waves from active seismic data and then estimate the HVSR for the fundamental mode. Based on the widespread application of the HVSR technique for the estimation of the impedance contrasts, we test the method of calculating active Rayleigh-wave HVSR in the presence of high-velocity contrasts and lateral variations. We also analyze the relationship between Rayleigh-wave fundamental-mode HVSR peak/trough frequencies and parameters of the subsurface model. The method is then applied to a field-data example.

## METHODOLOGY

In 2D active seismic surveys, P-SV wavefields are recorded by multichannel vertical and horizontal component geophones. The terms $f_H(t,x)$ and $f_V(t,x)$ represent the recorded horizontal and vertical component data, respectively, where $t$ is the time and $x$ is the offset. The terms $f_H(t,x)$ and $f_V(t,x)$ are a mixture of different wave types. Before calculating the HVSR, the fundamental mode of the Rayleigh-waves is first separated from the mixed wavefield records $f_H(t,x)$ and $f_V(t,x)$.

Rayleigh-wave mode separation can be performed using the high-resolution linear Radon transformation (HRLRT) (Luo et al., 2008, 2009), with which data are transformed from the time-offset ($t$-$x$) domain to the frequency-phase velocity ($f$-$v$) domain. The mode separation of Rayleigh waves using HRLRT basically requires three steps (Luo et al., 2009):

1) Transform the $t$-$x$ domain multichannel seismic records $f(t,x)$ into the $f$-$v$ domain $F(f,v)$ and generate the energy image in the $f$-$v$ domain.
2) Select spectra regions of one mode (fundamental mode) manually in the $f$-$v$ domain $F_0(f,v)$.
3) Transform the selected mode back to the $t$-$x$ domain $f_0(t,x)$.

Finally, $f_0(t,x)$ is the fundamental mode of the Rayleigh-wave seismic record. Luo et al. (2009) demonstrate the effectiveness of HRLRT as a means of separating and reconstructing multimode, dispersive Rayleigh-wave energy. The amplitude and phase can be preserved well using forward and inverse HRLRT (Hu et al., 2016). Accurate mode identification and selection are necessary to separate the fundamental mode.

Mode separation is carried out for both of the 2C data. We can obtain the horizontal $f_{H_0}(t,x)$ and vertical $f_{V_0}(t,x)$ components of the fundamental mode of Rayleigh waves. At the offset $x_0$, the Fourier spectra of the two components are $F_{H_0}(f,x_0)$ and $F_{V_0}(f,x_0)$. Then, the HVSR is estimated as

$$\mathrm{HVSR} = \frac{|F_{H_0}(f,x_0)|}{|F_{V_0}(f,x_0)|}, \tag{1}$$

where $F_{H_0}(f,x_0)$ is the Fourier spectra of the horizontal-component seismic trace relevant to fundamental-mode Rayleigh waves at the offset $x_0$ and $F_{V_0}(f,x_0)$ is the Fourier spectra of the vertical-component seismic trace relevant to fundamental-mode Rayleigh waves at the offset $x_0$.

For 1D layered earth models, the ellipticity of the fundamental Rayleigh waves is offset-independent. In other words, if the near-field effects can be ignored at far offsets, the estimated HVSR curves should be the same with different offsets for 1D models. Here, we compare the estimated HVSR curves with the theoretical HVSR curve, which is computed by solving the Rayleigh-wave

eigenproblem in the laterally homogeneous layered medium (e.g., Thomson, 1950; Haskell, 1953; Schwab and Knopoff, 1972; Abo-Zena, 1979; Kennett, 1983; Keilis-Borok et al., 1989; Chen, 1993; Hisada, 1994; Lai, 1998; Herrmann and Ammon, 2002). The theoretical HVSR is the ratio of the horizontal to vertical eigendisplacements of the fundamental mode of Rayleigh waves at the free surface (Appendix A).

## RAYLEIGH-WAVE HVSR ESTIMATION FOR MULTIMODAL DATA

In this section, we present a synthetic layered example (model 1, Table 1) to show the necessity and validity of separating the fundamental mode and then computing the HVSR of Rayleigh waves from active seismic data. The synthetic 2C seismic data are computed through finite-difference method solving the 2D elastic P-SV wave equations (Virieux, 1986; Xu et al., 2007; Zeng et al., 2011). We use a vertical point source, which is a 10 Hz (peak frequency) Ricker wavelet with a 100 ms delay, located at the free surface. For the finite-difference implementation, the model is uniformly discretized into $0.1 \times 0.1$ m cells so that the grid sample density is sufficient (at least 20 points per wavelength). The time step size is chosen as 0.02 ms to ensure that the finite-difference algorithm is numerically stable. The 2C seismic responses are recorded on the free surface with a 150-channel receiver array. The nearest offset is 1 m, with a subsequent 1 m receiver interval. Figure 1a and 1b shows the synthetic horizontal and vertical component data, respectively. The energy of Rayleigh waves is dominant in the horizontal and vertical component data.

**Table 1. Parameters of model 1.**

| Layer number | $V_P$ (m/s) | $V_S$ (m/s) | Density (g/cm$^3$) | $h$ (m) |
|---|---|---|---|---|
| 1 | 800 | 200 | 2.0 | 5 |
| 2 | 1200 | 400 | 2.0 | Infinite |

We obtained the dispersion images in the $f$-$v$ domain (Figure 1c and 1d) from the 2C multichannel records by the HRLRT, respectively. The energy of Rayleigh waves is nonnormalized in the images and indicates the different mode energy of the horizontal and vertical components, which is due to the different amplitudes between the horizontal and vertical particle motions of Rayleigh waves. The crosses and circles in Figure 1c and 1d represent the theoretical fundamental and first higher mode dispersion curves, respectively (Thomson, 1950; Haskell, 1953). The higher mode exists, although the energy is much lower than that of the fundamental mode.

We first calculated the HVSR directly from the synthetic 2C records of model 1. The results (Figure 2) show that if the mode separation is not performed, the HVSR curves calculated from active seismic data are not consistent with each other at different offsets for a 1D earth model. We separated the fundamental mode from the synthetic 2C data for model 1 (Figure 3). The energy of the Rayleigh-wave fundamental mode is concentrated at approximately 10–25 Hz for the horizontal and vertical components (Figure 3a and 3b), and the dashed yellow lines represent the selected fundamental mode range. Figure 3c and 3d shows the horizontal and vertical component data after the separation of the fundamental mode. Then, we computed HVSR from the fundamental-mode 2C records. The results (Figure 4) show that HVSR curves with different offsets

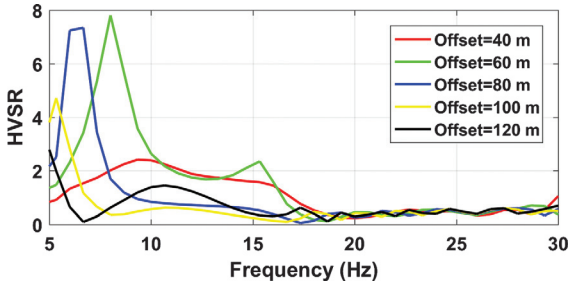


Figure 2. HVSR for model 1 computed from the 2C records in Figure 1a and 1b at different offsets.

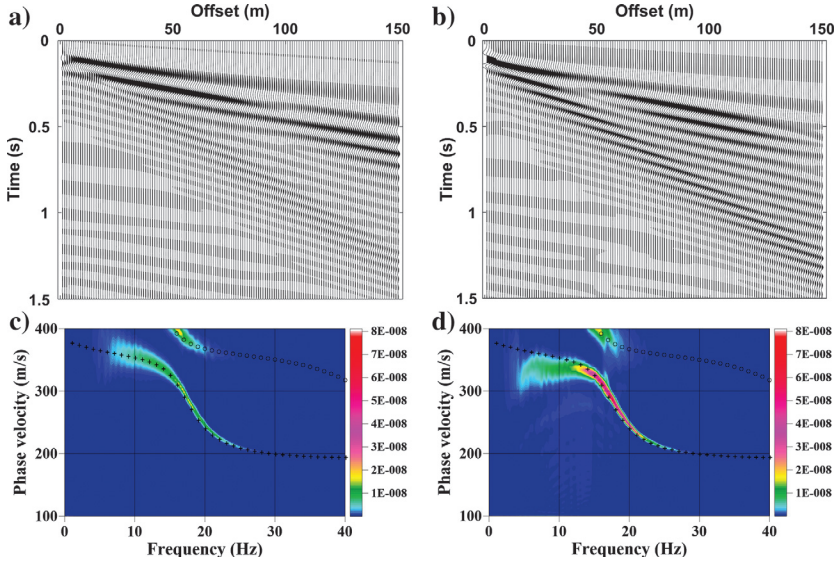


Figure 1. Synthetic (a) horizontal and (b) vertical component data for model 1 and (c and d) corresponding dispersion images generated by HRLRT. The crosses and circles in (c and d) represent the theoretical fundamental and first higher mode dispersion curves, respectively.

for the layered model 1 are very close to each other. The small differences between the estimated HVSR curves at different locations could be due to the calculation errors caused by the low energy of Rayleigh waves at lower frequencies (<12 Hz).

The theoretical HVSR curve (the dashed black line in Figure 4) is the ratio of the horizontal-to-vertical eigendisplacements of the fundamental mode of Rayleigh waves at the free surface, computed by solving the Rayleigh-wave eigenproblem in the laterally homogeneous layered medium (model 1). The small shift of peaks and troughs of the HVSR between the synthetic and theoretical data is due to the model discretization in the finite-difference modeling (as we illustrate in the next section).

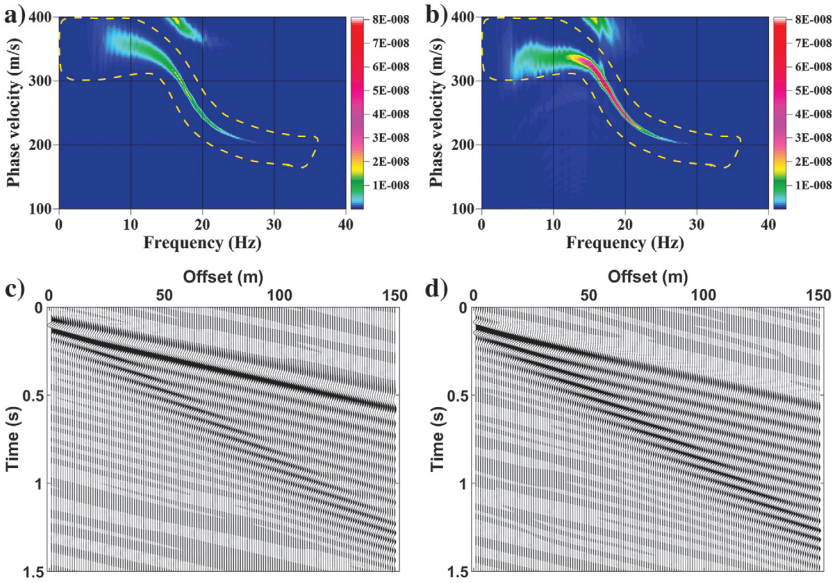


Figure 3. The selected single (fundamental) mode range (the dashed yellow lines) in the dispersion image of (a) horizontal and (b) vertical component data for model 1 and the separated fundamental mode of (c) horizontal and (d) vertical component data by the inverse HRLRT.

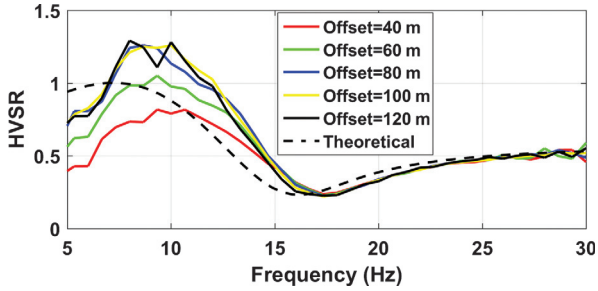


Figure 4. HVSR with different offsets for the layered model 1, estimated from the 2C records of the separated fundamental mode in Figure 3c and 3d. The theoretical HVSR curve for the fundamental mode of Rayleigh waves is computed by solving the Rayleigh eigenfunction in the laterally homogeneous layered medium (model 1). The small shift of peaks and troughs of the HVSR curves between the synthetic and theoretical data is due to the model discretization in the finite-difference modeling.

## RAYLEIGH-WAVE HVSR IN THE PRESENCE OF HIGH-VELOCITY CONTRASTS

The HVSR analysis technique is efficient for qualifying the impedance contrasts of layered-earth models, which usually exhibit the unconsolidated sediments over high-velocity bedrock. However, if there exists a strong velocity contrast in the earth model, Rayleigh-wave mode osculation happens. This phenomenon in Rayleigh-wave analysis may cause mode misidentification, so that a pure single mode cannot be separated for the estimation of HVSR.

We use a two-layer model (model 2, Table 2) to test the estimation of Rayleigh-wave HVSR in the presence of high-velocity contrasts. Parameters in the finite-difference modeling are the same as those for model 1. Figure 5a and 5b shows the synthetic horizontal and vertical component data for model 2, respectively. Figure 5c and 5d shows the corresponding spectra. The crosses and circles represent the theoretical fundamental and first higher mode dispersion curves, respectively (Thomson, 1950; Haskell, 1953). In Figure 5c and 5d, we noted that mode osculation occurs at approximately 13 Hz and the energy peak shifts from the fundamental to the first higher mode for the horizontal and vertical component data. In this case, it is not possible to perfectly separate the fundamental mode by looking at the spectra. Here, we select the fundamental mode using the information provided by the theoretical fundamental mode dispersion curve (the dashed yellow lines in Figure 5c and 5d). The separated fundamental mode of the horizontal and vertical component data is shown in Figure 5e and 5f. The estimated HVSR from the 2C records of the separated fundamental mode is shown in Figure 6. The HVSR curves with different offsets for the layered model 2 are very close to each other (Figure 6). There are differences between the synthetic and theoretical data at lower frequencies (<13 Hz). This is because there is almost no energy for the fundamental mode of Rayleigh waves at frequencies lower than that of the osculation point. We could not obtain the accurate Rayleigh-wave HVSR at lower frequencies from the active-seismic records in the presence of high-velocity contrasts.

In this synthetic example, the separation of the fundamental mode in the presence of high-velocity contrasts is based on the accurate selection of the fundamental mode range along the theoretical fundamental dispersion curve. In real-world applications, however, the theoretical dispersion curve is unknown. Mode misidentification could be unavoidable, and the selected single mode could be an impure fundamental mode that contains the high mode energy at lower

**Table 2. Parameters of model 2.**

| Layer number | $V_P$ (m/s) | $V_S$ (m/s) | Density (g/cm$^3$) | $h$ (m) |
|---|---|---|---|---|
| 1 | 800 | 180 | 1.9 | 5 |
| 2 | 1500 | 500 | 2.0 | Infinite |

frequencies (Figure 7). With the 2C records of the separated impure fundamental mode (Figure 7c and 7d), HVSR curves are estimated in Figure 8. HVSR curves (Figure 8) at higher frequencies (>13 Hz) estimated from the impure fundamental mode are similar to those in Figure 6. The mode energy misidentification on account of mode osculation has no influence on the estimation of HVSR at frequencies higher than that of the osculation point. The estimated HVSR at lower frequencies (<13 Hz) is the result of the Rayleigh-wave first higher mode, which is different from the theoretical HVSR of the fundamental mode of Rayleigh waves.

These synthetic results show that in the presence of high-velocity contrasts, mode osculation has no influence on the estimation of Rayleigh-wave HVSR at frequencies higher than that of the osculation point, where HVSR troughs appear for the near-surface two-layer model. We can hardly obtain the accurate HVSR at frequencies lower than that of the osculation point, where HVSR peaks appear for the two-layer model, either because of the lack of energy of the fundamental mode or because of the existence of energy of the first higher mode.

The HVSR peak and trough frequencies are linked to parameters of the earth model (e.g., Tuan et al., 2011). Figure 9a shows different theoretical HVSR curves of the Rayleigh-wave fundamental mode for the two-layer model 2 with various thicknesses of the first layer. With the increasing thicknesses, the HVSR peaks and troughs shift from high frequencies to low frequencies. The shift of the HVSR curve for a thickness variation of 0.5 m at different depths is shown in Figure 9b. At shallow depths, a 0.5 m change of thickness of the first layer produces a significant shift of the HVSR trough. This example shows that HVSR peak and trough frequencies are very sensitive to the depth of bedrock in near-surface models and that sensitivity to depth is higher for shallow depths.

Let us go back to the shift of the HVSR peaks and troughs between the synthetic and theoretical data (Figures 4, 6, and 8). In our finite-difference modeling, the grid step for the model discretization is 0.1 m, which means that the layer thickness for the synthetic data could be different compared to the theoretical data because of the model discretization. This leads to the shift of HVSR curves between the synthetic and theoretical data. This phenomenon of shifting can also be observed by comparing the dispersion energy generated from synthetic data and the theoretical dispersion curve (Figure 5c and 5d for model 2). We use another model (Figure 10) to show that HVSR troughs estimated from the synthetic data can be almost the same with the theoretical one if the discretization can be neglected in comparison to the interface depth. The model in Figure 10 has a deep interface. The estimated HVSR troughs are basically the same as the theoretical one. HVSR peaks are not obtained due to the high-velocity contrast in the model. The

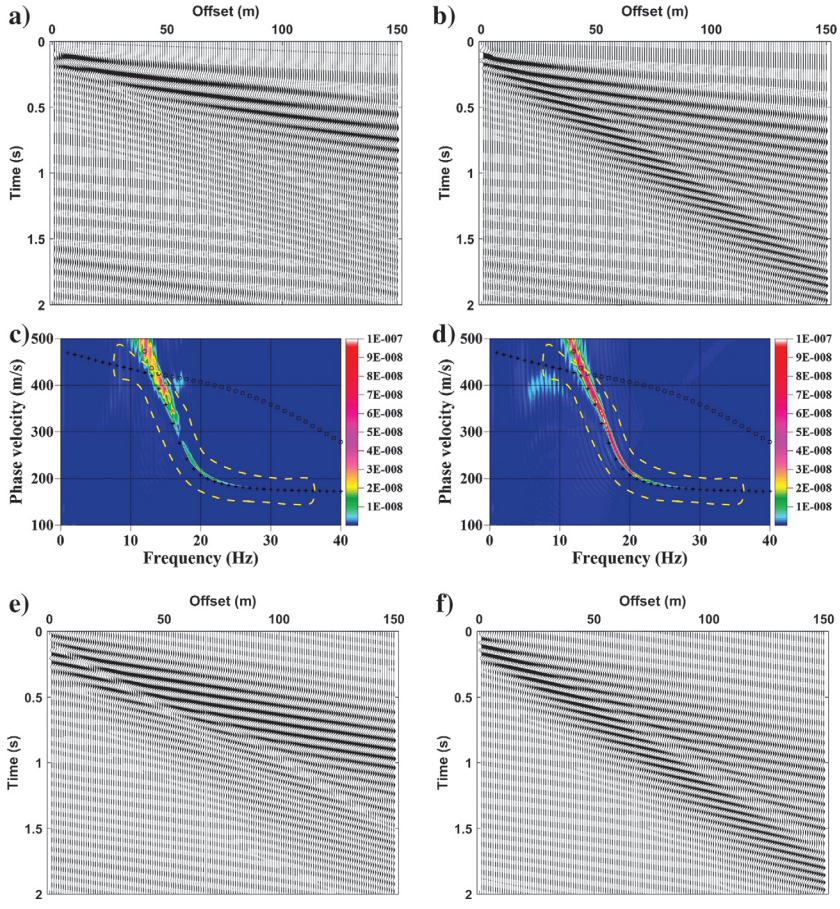


Figure 5. (a and b) Synthetic horizontal and vertical component data for model 2. (c and d) The selected single (fundamental) mode range (the dashed yellow lines) in the dispersion image of horizontal and vertical component data. (e and f) The separated fundamental mode of horizontal and vertical component data. The crosses and circles in (c and d) represent the theoretical fundamental and first higher mode dispersion curves, respectively.

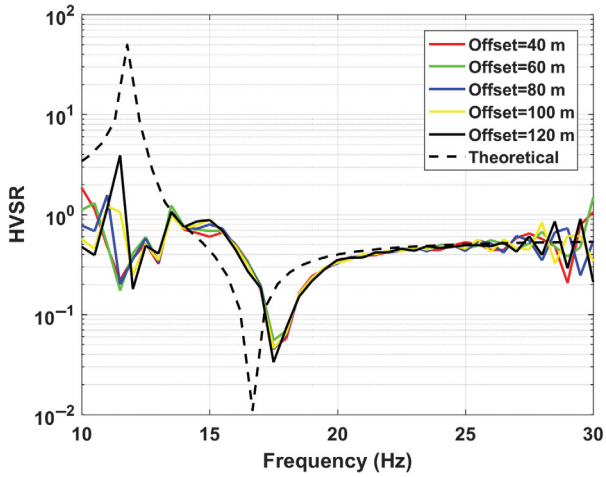


Figure 6. HVSR with different offsets for the layered model 2, estimated from the 2C records of the separated fundamental mode in Figure 5e and 5f. The theoretical HVSR curve for the fundamental mode of Rayleigh waves is computed by solving the Rayleigh eigenfunction in the laterally homogeneous layered medium (model 2). The shift of the HVSR troughs between the synthetic and theoretical data is due to the model discretization in the finite-difference modeling.

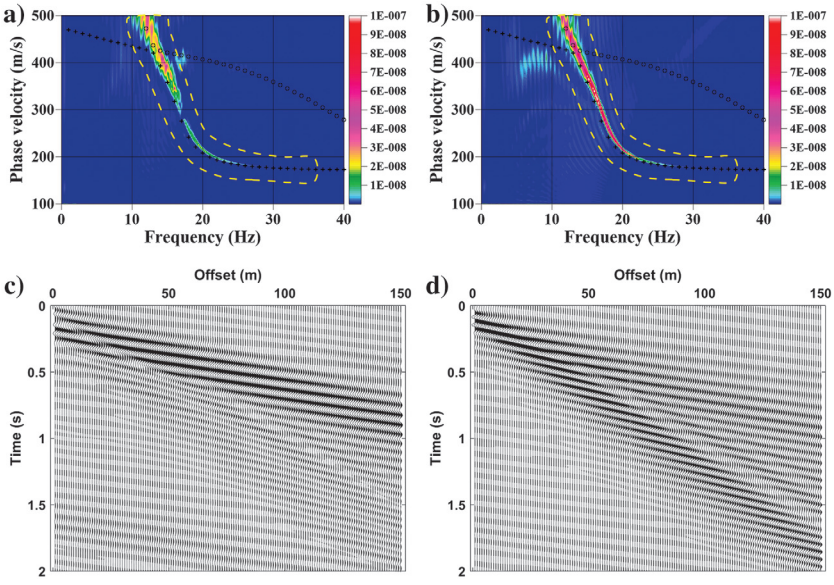


Figure 7. (a and b) The selected mode range regardless of the mode osculation (the dashed yellow lines) in the dispersion image of horizontal and vertical component data. (c and d) The separated impure mode of horizontal and vertical component data. The crosses and circles in (a and b) represent the theoretical fundamental and first higher mode dispersion curves, respectively.

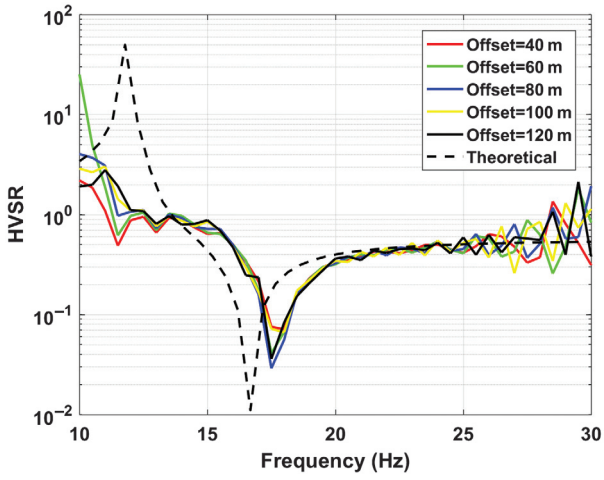


Figure 8. HVSR with different offsets for the layered model 2, estimated from the 2C records of the separated impure fundamental mode in Figure 7c and 7d. The theoretical HVSR curve is of the fundamental mode of Rayleigh waves, computed by solving the Rayleigh eigenfunction in the laterally homogeneous layered medium (model 2). The shift of the HVSR troughs between the synthetic and theoretical data is due to the model discretization in the finite-difference modeling.

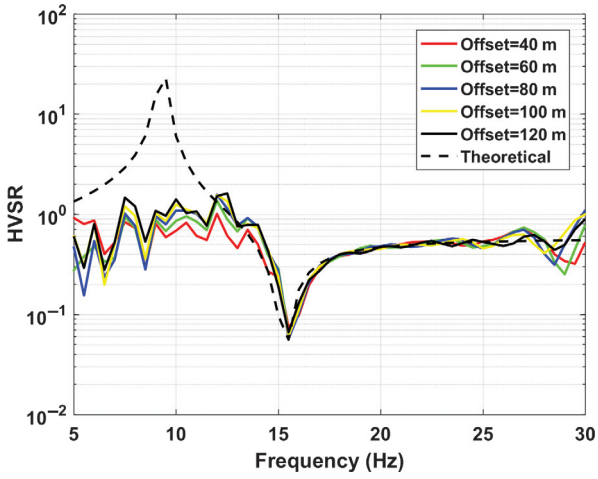


Figure 10. HVSR for the model with deeper layer interface. The thickness of the top layer is 15 m. The values of $V_P$, $V_S$, and density in the top layer are 1900 m/s, 480 m/s, and 2.1 g/cm$^3$, respectively. In the half-space, the values of $V_P$, $V_S$, and density are 4000 m/s, 1500 m/s, and 2.3 g/cm$^3$, respectively. For this model, HVSR troughs estimated from the synthetic data are basically the same with the theoretical one. HVSR peaks are not obtained due to the high-velocity contrast.

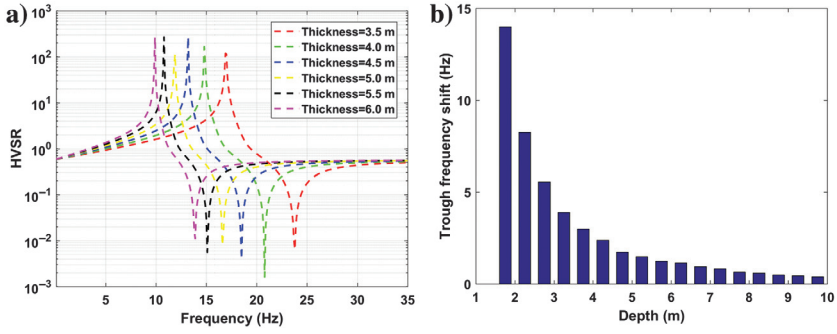


Figure 9. (a) Theoretical HVSR of the fundamental mode of Rayleigh waves for the layered model 2 with various thicknesses of the first layer, computed by solving the Rayleigh eigenfunction in the laterally homogeneous layered medium. (b) The shift of the HVSR curve for a thickness variation of 0.5 m at different depths of model 2.

comparison makes sense only at frequencies higher than the osculation frequency.

## RAYLEIGH-WAVE HVSR IN LATERALLY VARYING MEDIA

A slope synthetic model (Figure 11) is used to test for the effect of lateral variations in the estimation of Rayleigh-wave HVSR. The model consists of two layers (the $V_P$, $V_S$, and densities are the same with model 2), and there is a dipping interface that makes the thickness of the first layer vary linearly from 4 to 5 m. The parameters in the finite-difference modeling are the same as those for model 2. Seismic signals are recorded on the free surface with a 49-channel

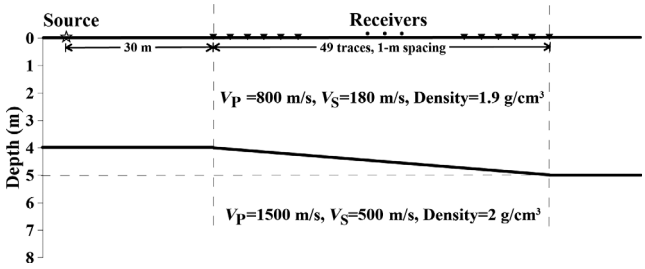


Figure 11. Illustration of a model with lateral variations. The model consists of two layers ($V_P$, $V_S$, and densities are the same with model 2), and there is a sloping interface that makes the thickness of the first layer increases gradually from 4 to 5 m (from the left to the right). Seismic responses are recorded on the free surface with a 49-channel 2C receiver array, which is right above the sloping interface. The nearest offset is 30 m, with a subsequent 1 m receiver interval.

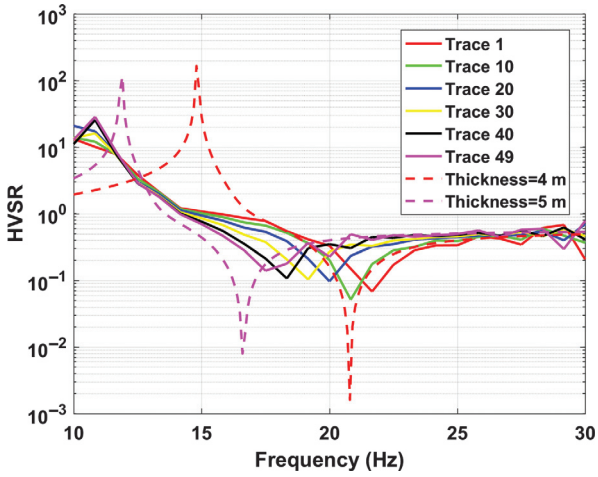


Figure 13. HVSR at different traces for the slope model in Figure 11, estimated from the 2C records of the separated fundamental mode in Figure 12e and 12f. From trace 1 to 49, the thickness of the first layer increases from 4 to 5 m. The dashed red and magenta lines represent the theoretical HVSR curves for the two-layer model with 4 and 5 m thickness of the first layer, respectively.

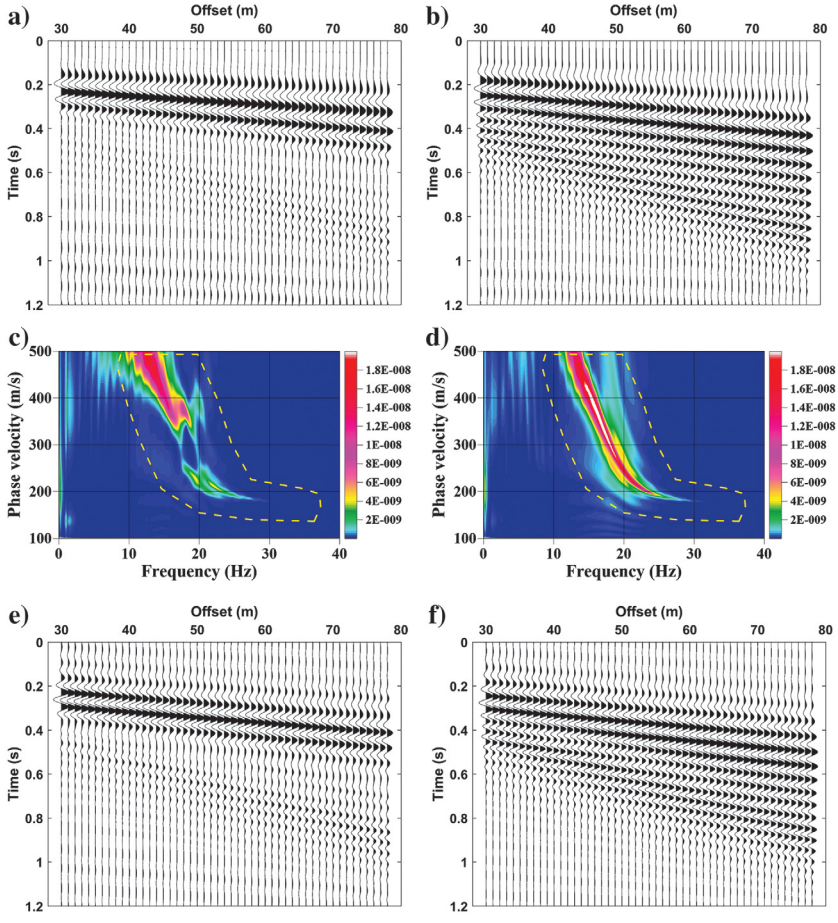


Figure 12. (a and b) Synthetic horizontal and vertical component data for the slope model in Figure 11. (c and d) The selected single (fundamental) mode range (the dashed yellow lines) in the dispersion image of horizontal and vertical component data. The spectra are restricted in the S-wave velocity range of the true model (180 m/s in the top layer and 500 m/s in the half-space). (e and f) The extracted mode of horizontal and vertical component data.

2C receiver array, which is right above the dipping interface. The nearest offset is 30 m (to reduce near-field effects, as illustrated in Pan et al., 2013), with a subsequent 1 m receiver interval. Figure 12a and 12b shows the synthetic horizontal and vertical component data for the slope model, respectively. We show the corresponding spectra in Figure 12c and 12d. The dashed yellow lines (Figure 12c and 12d) represent the selected fundamental mode range. The extracted mode of horizontal and vertical component data is shown in Figure 12e and 12f.

The estimated HVSR curves for the slope model are different at different traces (Figure 13). The HVSR peaks from the synthetic data at low frequencies are incorrect due to the lack of fundamental mode energy in the presence of strong velocity contrasts (as discussed in the previous section). However, the HVSR troughs from synthetic data lay between the two theoretical HVSR curves of the two-layer model with the 4 and 5 m thicknesses of the first layer. From traces 1–49, the HVSR troughs shift from high frequencies to low frequencies, with the increasing thickness of the first layer. This indicates that HVSR estimation can be carried out in the presence of lateral variations and the HVSR estimated from the fundamental Rayleigh-wave mode contains the information on bedrock depth lateral variations, which can be used to constrain the reconstruction of 2D subsurface structures.

## HVSR PEAK/TROUGH FREQUENCIES VERSUS MODEL PARAMETERS

The fundamental Rayleigh-wave HVSR exhibits a peak at the low frequency and a trough at the high frequency for models with a soft layer over a stiff half-space (Figure 9). The peak and trough frequencies are strongly linked to the model parameters. To evaluate the possibility of using a simple relation for the interpretation of the HVSR results, we carried out a Monte Carlo simulation computing the frequency of fundamental-mode HVSR peak and trough for 5000 randomly generated models. Each model contains a single soil layer (S-wave velocity $V_{S1}$ varies from 80 to 600 m/s) over a stiff half-space (S-wave velocity $V_{S2}$ varies from 300 to 2000 m/s), in which we make sure the S-wave velocity in the first layer is lower than the half-space. The thickness ($h$) of the soil layer varies from 0.5 to 50 m. The Poisson's ratio and density are constants (0.43 and 1.9 g/cm$^3$ in the first layer and 0.40 and 2.0 g/cm$^3$ in the half-space, respectively). The HVSR peak and trough of the Rayleigh-wave fundamental mode are computed by solving the Rayleigh eigenfunction. For each model, we apply a similar empirical equation in a passive HVSR analysis (Nakamura, 1989):

$$f = \frac{1}{k}\frac{V_{S1}}{h}, \tag{2}$$

where $V_{S1}$ and $h$ represent the S-wave velocity and thickness of the soil layer, respectively, $f$ is the peak/trough frequency, and $k$ is the coefficient.

The plots of the peak and trough frequencies with respect to $V_{S1}/h$ (Figure 14) show that the coefficient $k$ is not constant in the relationship between the peak/trough frequencies of the fundamental-mode Rayleigh-wave HVSR and the model parameter $V_{S1}/h$. The value of $k$ is indeed influenced by the velocity contrast $V_{S1}/V_{S2}$ ($V_{S2}$ is the S-wave velocity of the stiff half-space). For low $V_{S1}/V_{S2}$ (higher velocity contrasts), the value of $k$ decreases. The value of $k$ can vary from 20 to 2.5 for the HVSR peak frequencies (Figure 14a). If the velocity contrasts are extremely strong ($V_{S1}/V_{S2} < 0.2$), $k$ tends toward 4.0 for the peak frequencies. For the trough frequencies, $k$ is confined in a range from 2.5 to 2.0 (Figure 14b). This indicates that the trough frequencies have lower sensitivity to the velocity contrast and can therefore be used to estimate the interface depth with only knowledge of $V_{S1}$ (equation 2).

## FIELD-DATA EXAMPLE

We present an example of Rayleigh-wave HVSR estimation from real-world 2C data. The field data were collected at the Boise Hydrogeophysical Research Site (BHRS), which is an experimental well field located on a gravel bar adjacent to the Boise River, 15 km from downtown Boise, Idaho, USA. Down-hole seismic sur-

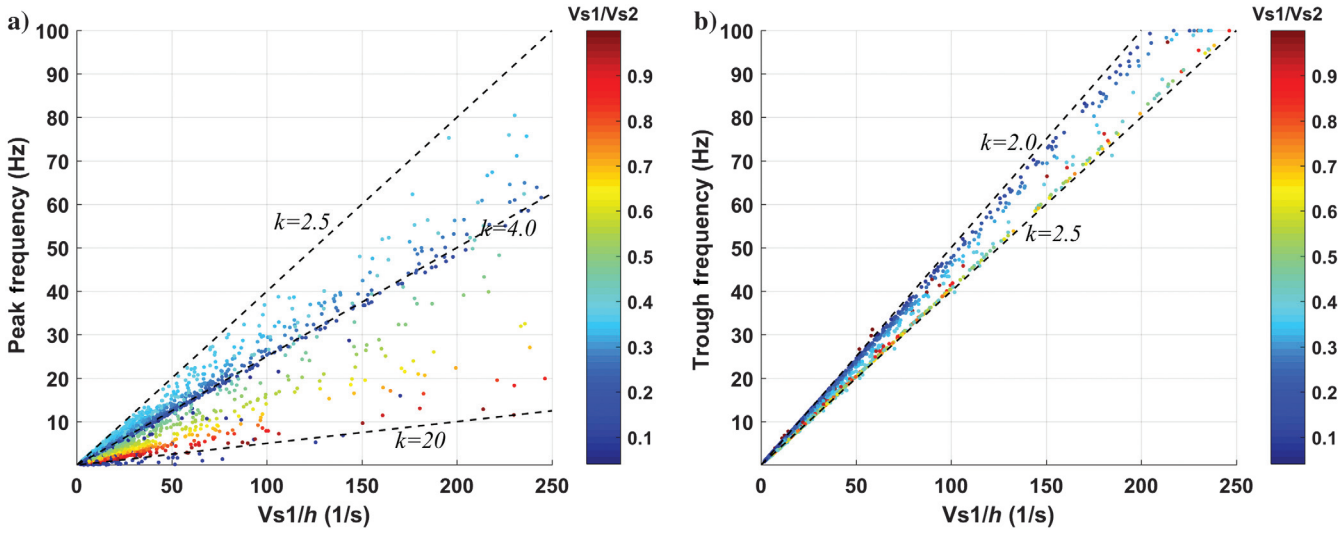


Figure 14. (a) Peak/(b) trough frequencies of fundamental-mode Rayleigh-wave HVSR versus the model parameter $V_{S1}/h$. The color scale represents the value of $V_{S1}/V_{S2}$, which shows the velocity contrasts between the soil layer and the half-space. The term $k$ is the coefficient in equation 2.

veys (Michaels and McCabe, 1999) and surface-wave dispersion analysis at the BHRS present the S-wave velocities above a depth of 20 m, which show that this area can be roughly divided into two layers with strong velocity contrasts. The $V_S$ of the first layer is approximately 150 m/s with 2–4 m thickness, and the $V_S$ of the half-space is more than 500 m/s. In the data acquisition, 24 vertical component geophones (4.5 Hz) and 24 horizontal component geophones (4.5 Hz, inline) were used. The source was a 5 kg hammer vertically impacting a metal plate. The receiver interval was 1.25 m with the 12.5 m nearest source-to-receiver offset. Rayleigh waves are dominant in the recorded 2C data (Figure 15).

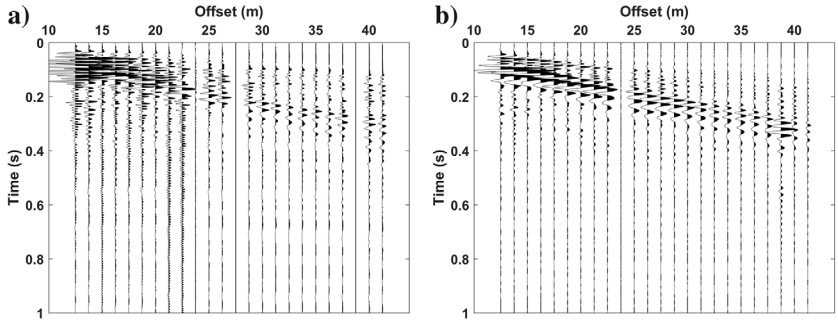


Figure 15. Field data at the BHRS: (a) horizontal (in-line) component, and (b) vertical component.

We first calculated the HVSR directly from the 2C records without mode separation. The results of the first six traces are shown in Figure 16. The HVSR curves are disturbed and appear disorderly and unsystematic at high frequencies (>20 Hz). Then, we separated the fundamental mode (Figure 17) and calculated the HVSR again (Figure 18). In Figure 17a and 17b, higher modes are visible and it is possible to separate them at least at a high frequency. With the fundamental mode of Rayleigh waves only, the HVSR troughs stand out at approximately 22 Hz for the first 12 traces (Figure 18). HVSR curves with larger offsets (traces 13–24) are more noisy and less consistent with each other. This could be caused by the lateral variations or the low signal-to-noise ratio at far traces of the horizontal components. HVSR peaks at low frequencies estimated from field data could not be derived from the active fundamental Rayleigh waves because the energy is very weak at frequencies lower than 15 Hz (Figure 17a and 17b).

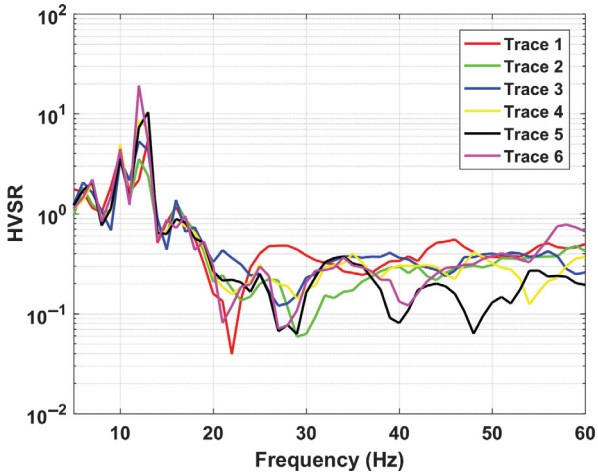


Figure 16. HVSR at traces 1–6 of the field data, directly calculated from the 2C records (Figure 15) without mode separation.

We applied equation 2 to the field data for the depth estimation of the soil layer. The HVSR trough frequency for the field data at trace 5 (Figure 18) is approximately 22 Hz. With $V_{S1} = 150$ m/s and $k$ between 2.0 and 2.5, the depth of the soil layer is 2.7–3.4 m using equation 2. The estimated soil layer depth is consistent with the borehole results (Michaels and McCabe, 1999).

## DISCUSSION

We have verified that it is necessary to isolate the fundamental mode of Rayleigh waves before calculating the HVSR. The accurate mode identification and selection are essential to separate the fundamental mode using HRLRT. If there is mode osculation caused by the high-velocity contrast, the HVSR peak of the fundamental mode occurs at a frequency lower than the osculation frequency, and the trough occurs at a frequency higher than the osculation frequency. Therefore, the estimated HVSR troughs are impervious in the presence of mode osculation.

In the synthetic data, there is a small shift between the estimated HVSR and theoretical one. We have illustrated that it is due to the model discretization in the finite-difference modeling and the high sensitivity of HVSR peak and trough frequencies to the shallow depth of the bedrock.

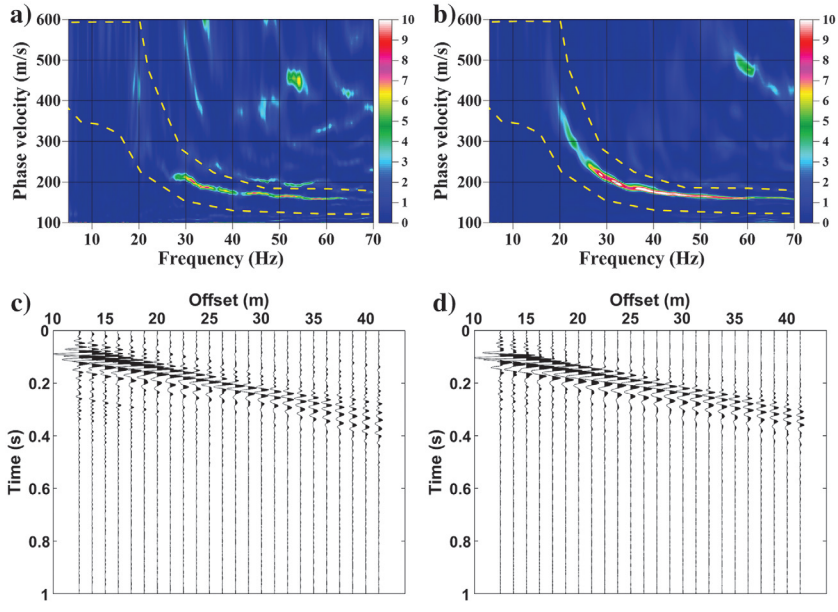


Figure 17. (a and b) Dispersion images of the horizontal and vertical component field data (Figure 15) and the selected single (fundamental) mode range (the dashed yellow lines). (c and d) The separated fundamental mode of horizontal and vertical component data.

We have tried to use different discretization steps (0.5, 0.2, 0.1, and 0.05 m, the smaller step, the greater amount of computation) for the seismic modeling of model 2. Results show that the shift becomes smaller with smaller grid step, but the difference cannot be eliminated because of the approximate numerical solution of the finite-difference modeling. For model 2, if we set the depth of the first layer a little larger than 5 m in the modeling (5.1 m, for example, which can approximately make the thickness of the first layer be equivalent to 5 m after discretization), the estimated HVSR curves and theoretical one show great consistency.

In real-world applications, HVSR troughs without mode separation are disturbed by high-frequency interference waves or noises (Figure 16). HVSR peaks could not be derived from the fundamental mode because the energy of active Rayleigh waves is very weak at the low frequency. With the existence of mode osculation, the higher mode Rayleigh waves can be dominant at the peak frequency for the model with high-velocity contrast, which are also polarized at the fundamental frequency of resonance of the sediments (Fäh et al., 2001) and can explain the peak of the estimated HVSR curve (Figure 18). Generally, using a light seismic source as those that are mainly used for shallow near-surface investigations, it is difficult to obtain the low-frequency (<10 Hz) energy. Therefore, estimating the HVSR trough from real data is more easily achieved than peak estimation.

The choice of the observation system (the nearest offset, the receiver interval, and spread length) in the field data acquisition is similar to the optimum layout for MASW (Park et al., 1999) because generating a good dispersion image from raw data is a precondition for mode extraction and separation. More field data are needed and should be tested with this method in the future.

We only analyzed the fundamental mode HVSR of Rayleigh waves. The same method could be applied more generally to any single mode (e.g., the first high mode). The Rayleigh-wave HVSR peak and trough frequencies are highly sensitive to the parameters of the near-surface model. It will be of great significance to investigate shallow subsurface 2D structures by inverting the HVSR peak and trough and/or its entire spectrum derived from active seismic data, or joint analysis with dispersion data (e.g., Castellaro, 2016) from the MASW method.

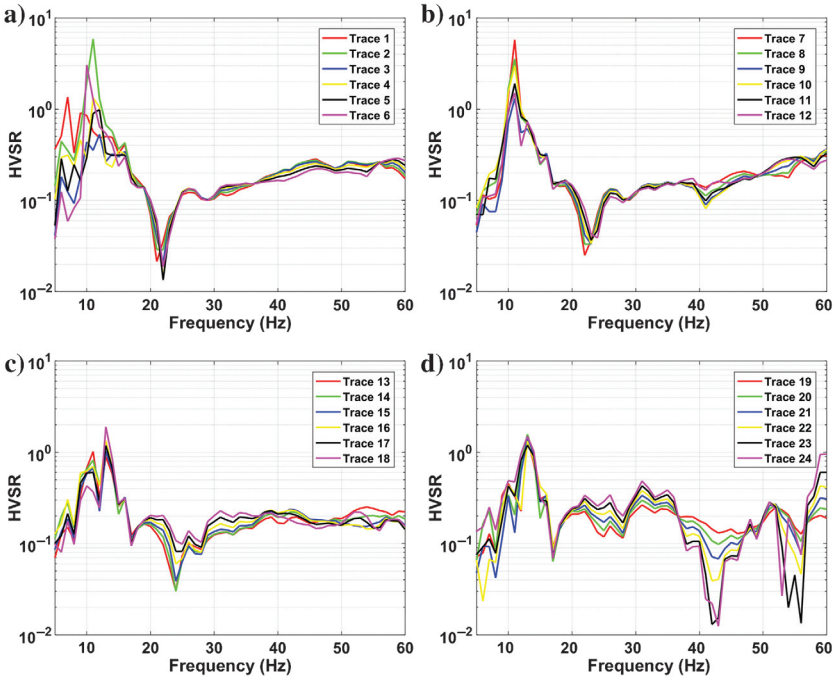


Figure 18. HVSR at different traces of the field data, estimated from the 2C records of the separated fundamental mode in Figure 17c and 17d.

## CONCLUSION

The different mode energy information from the horizontal and vertical components in Rayleigh-wave analysis prompted us to apply the HVSR method to multicomponent active-seismic data. The recorded active-seismic signals are a mixture of various wave types; thus, we first isolate the fundamental mode of Rayleigh waves using a high-resolution spectral estimator, and then we calculate the HVSR. The mode separation is implemented in the $f$-$v$ domain by the HRLRT, which requires multiple channel records to generate dispersion energy maps of Rayleigh waves. Being able to isolate the fundamental mode in the frequency band of interest for HVSR estimation is a necessary condition. The HVSR is hence reliable only in the frequency band within which the fundamental mode can be reliably selected. The estimated Rayleigh-wave HVSR curve after mode separation is consistent with the theoretical HVSR curve computed by solving the Rayleigh-wave eigenproblem.

For simple models made of a soft layer underlying a stiff half-space, the HVSR peak is very sensitive to the interface depth and velocity contrast, whereas the trough frequency is sensitive to interface depth only and it is poorly affected by the velocity contrast. A simple relationship has been established between the fundamental-mode Rayleigh-wave HVSR trough frequencies and the model parameters. Because the estimation of the trough from real data is also more reliable than peak estimation, the HVSR trough is a good candidate for adding useful information in the dispersion inversion and interpretation.

## ACKNOWLEDGMENTS

The authors greatly appreciate the comments and suggestions from the editor J. Shragge, the assistant editor J. Etgen, the associate editor G. Tsoflias, and three anonymous reviewers that significantly improved the quality of the manuscript. The authors thank J. Bradford, C. Shen, and the students in the Center for Geophysical Investigation of the Shallow Subsurface (CGISS), Boise State University, for their generous help in the field data acquisition. The authors also thank Z. Xu and C. Comina for helpful discussions and suggestions. This study is supported by the National Natural Science Foundation of China under grant nos. 41774115 and 41830103 and the China Postdoctoral Science Foundation under grant no. 2019M652061. The first author also thanks the China University of Geosciences in Wuhan and the China Scholarship Council for the financial support to conduct this research.

## DATA AND MATERIALS AVAILABILITY

Data associated with this research are available and can be obtained by contacting the corresponding author.

## APPENDIX A

## CALCULATION OF THE THEORETICAL HVSR CURVE

The theoretical HVSR curve (ellipticity) of fundamental-mode Rayleigh waves is calculated by solving the Rayleigh-wave eigenproblem in the laterally homogeneous layered medium. Computing the dispersion curves and their corresponding eigenfunctions for a stratified earth model is fundamental in studying surface waves. A large number of studies have been carried out since Thomson and Haskell's pioneering studies (e.g., Thomson, 1950; Haskell, 1953; Schwab and Knopoff, 1972; Abo-Zena, 1979; Kennett, 1983; Keilis-Borok et al., 1989; Chen, 1993; Hisada, 1994; Lai, 1998; Herrmann and Ammon, 2002). The main algorithms we used are based on Hisada and Lai's studies (Hisada, 1994; Lai, 1998).

We can obtain the horizontal $r_H(f, n, z)$ and vertical $r_V(f, n, z)$ eigendisplacements of Rayleigh waves after solving the Rayleigh-wave eigenproblem in a layered model, where $f$ represents the frequency, $n$ ($n = 0$, 1, 2, etc.) designates the $n$th mode, and $z$ represents the depth. Thus, the theoretical HVSR of the fundamental-mode Rayleigh waves is calculated as

$$\mathrm{HVSR}_{\mathrm{theoretical}} = \frac{r_H(f, n = 0, z = 0)}{r_V(f, n = 0, z = 0)}, \tag{A-1}$$

where $r_H(f, n = 0, z = 0)$ and $r_V(f, n = 0, z = 0)$ are the horizontal and vertical eigendisplacements of the fundamental mode of Rayleigh waves at the free surface, respectively.

## REFERENCES


Abo-Zena, A. M., 1979, Dispersion function computations for unlimited frequency values: Geophysical Journal of the Royal Astronomical Society, **58**, 91–105, doi: 10.1111/j.1365-246X.1979.tb01011.x.

Arai, H., and K. Tokimatsu, 2004, S-wave velocity profiling by inversion of microtremor H/V spectrum: Bulletin of the Seismological Society of America, **94**, 53–63, doi: 10.1785/0120030028.

Bignardi, S., A. Mantovani, and N. A. Zeid, 2016, Open HVSR: Imaging the subsurface 2D/3D elastic properties through multiple HVSR modeling and inversion: Computers and Geosciences, **93**, 103–113, doi: 10.1016/j.cageo.2016.05.009.

Boaga, J., G. Cassiani, C. L. Strobbia, and G. Vignoli, 2013, Mode misidentification in Rayleigh waves: Ellipticity as a cause and a cure: Geophysics, **78**, no. 4, EN17–EN28, doi: 10.1190/geo2012-0194.1.

Bonnefoy-Claudet, S., A. Köhler, C. Cornou, M. Wathelet, and P.-Y. Bard, 2008, Effects of love waves on microtremor H/V ratio: Bulletin of the Seismological Society of America, **98**, 288–300, doi: 10.1785/0120070063.

Castellaro, S., 2016, The complementarity of H/V and dispersion curves: Geophysics, **81**, no. 6, T323–T338, doi: 10.1190/geo2015-0399.1.

Chen, X., 1993, A systematic and efficient method of computing normal modes for multilayered half-space: Geophysical Journal International, **115**, 391–409, doi: 10.1111/j.1365-246X.1993.tb01194.x.

Dal Moro, G., and F. Ferigo, 2011, Joint analysis of Rayleigh- and Love-wave dispersion: Issues, criteria and improvements: Journal of Applied Geophysics, **75**, 573–589, doi: 10.1016/j.jappgeo.2011.09.008.

Fäh, D., F. Kind, and D. Giardini, 2001, A theoretical investigation of average H/V ratios: Geophysical Journal International, **145**, 535–549, doi: 10.1046/j.0956-540x.2001.01406.x.

Fäh, D., F. Kind, and D. Giardini, 2003, Inversion of local S-wave velocity structures from average H/V ratios and their use for the estimation of site-effects: Journal of Seismology, **7**, 449–467, doi: 10.1023/B:JOSE.0000005712.86058.42.

Foti, S., S. Parolai, D. Albarello, and M. Picozzi, 2011, Application of surface-wave methods for seismic site characterization: Surveys in Geophysics, **32**, 777–825, doi: 10.1007/s10712-011-9134-2.

Gao, L., J. Xia, and Y. Pan, 2014, Misidentification caused by leaky surface wave in high-frequency surface wave method: Geophysical Journal International, **199**, 1452–1462, doi: 10.1093/gji/ggu337.

García-Jerez, A., J. Piña-Flores, F. J. Sánchez-Sesma, F. Luzón, and M. Perton, 2016, A computer code for forward computation and inversion of the H/V spectral ratio under the diffuse field assumption: Computers and Geosciences, **97**, 67–78, doi: 10.1016/j.cageo.2016.06.016.

Gribler, G., and T. D. Mikesell, 2016, Joint inversion of H/V spectral ratios and phase-velocity dispersion with active seismic data: 86th Annual International Meeting, SEG, Expanded Abstracts, 4977–4982, doi: 10.1190/segam2016-13864369.1.

Haskell, N. A., 1953, The dispersion of surface waves on multilayered media: Bulletin of the Seismological Society of America, **43**, 17–34.

Haskell, N. A., 1960, Crustal refection of plane SH waves: Journal of Geophysical Research, **65**, 4147–4150, doi: 10.1029/JZ065i012p04147.

Herrmann, R. B., and C. J. Ammon, 2002, Computer programs in seismology: Surface waves, receiver functions and crustal structure, version 3.20: Saint Louis University.

Hisada, Y., 1994, An efficient method for computing Green's functions for a layered half-space with sources and receivers at close depths: Bulletin of the Seismological Society of America, **84**, 1456–1472.

Hobiger, M., C. Cornou, M. Wathelet, G. Di Giulio, B. Knapmeyer-Endrun, F. Renalier, P.-Y. Bard, A. Savvaidis, S. Hailemikael, B. N. Le, M. Ohrnberger, and N. Theodoulidis, 2013, Ground structure imaging by inversions of Rayleigh wave ellipticity: Sensitivity analysis and application to European strong-motion sites: Geophysical Journal International, **192**, 207–229, doi: 10.1093/gji/ggs005.

Hu, Y., L. Wang, F. Cheng, Y. Luo, C. Shen, and B. Mi, 2016, Ground-roll noise extraction and suppression using high-resolution linear Radon transform: Journal of Applied Geophysics, **128**, 8–17, doi: 10.1016/j.jappgeo.2016.03.007.

Ikeda, T., T. Matsuoka, T. Tsuji, and T. Nakayama, 2015, Characteristics of the horizontal component of Rayleigh waves in multimode analysis of surface waves: Geophysics, **80**, no. 1, EN1–EN11, doi: 10.1190/geo2014-0018.1.

Kawase, H., S. Matsushima, T. Satoh, and F. J. Sánchez-Sesma, 2015, Applicability of theoretical horizontal-to-vertical ratio of microtremors based on the diffuse field concept to previously observed data: Bulletin of the Seismological Society of America, **105**, 3092–3103, doi: 10.1785/0120150134.

Keilis-Borok, V. I., A. L. Levshin, T. B. Yanovskaya, A. V. Lander, B. G. Bukchin, M. P. R. Barmin, L. I. Ratnikova, and E. N. Its, 1989, Seismic surface waves in a laterally inhomogeneous earth: Kluwer Academic Publishers.

Kennett, B. L. N., 1983, Seismic wave propagation in stratified media: Cambridge University Press.

Lachet, C., and P.-Y. Bard, 1994, Numerical and theoretical investigations on the possibilities and limitations of Nakamura's technique: Journal of Physics of the Earth, **42**, 377–397, doi: 10.4294/jpe1952.42.377.

Lai, C. G., 1998, Simultaneous inversion of Rayleigh phase velocity and attenuation for near-surface site characterization: Ph.D. dissertation, Georgia Institute of Technology.

Lontsi, A. M., F. J. Sánchez-Sesma, J. C. Molina-Villegas, M. Ohrnberger, and F. Kruger, 2015, Full microtremor H/V (z, f) inversion for shallow subsurface characterization: Geophysical Journal International, **202**, 298–312, doi: 10.1093/gji/ggv132.

Lunedei, E., and D. Albarello, 2015, Horizontal-to-vertical spectral ratios from a full-wavefield model of ambient vibrations generated by a distribution of spatially correlated surface sources: Geophysical Journal International, **201**, 1142–1155, doi: 10.1093/gji/ggv046.

Luo, Y., J. Xia, R. D. Miller, Y. Xu, J. Liu, and Q. Liu, 2008, Rayleigh-wave dispersive energy imaging by high-resolution linear Radon transform: Pure and Applied Geophysics, **165**, 903–922, doi: 10.1007/s00024-008-0338-4.

Luo, Y., J. Xia, R. D. Miller, Y. Xu, J. Liu, and Q. Liu, 2009, Rayleigh-wave mode separation by high-resolution linear Radon transform: Geophysical Journal International, **179**, 254–264, doi: 10.1111/j.1365-246X.2009.04277.x.

Malischewsky, P. G., and F. Scherbaum, 2004, Love's formula and H/V-ratio (ellipticity) of Rayleigh waves: Wave Motion, **40**, 57–67, doi: 10.1016/j.wavemoti.2003.12.015.

Mi, B., J. Xia, C. Shen, and L. Wang, 2018, Dispersion energy analysis of Rayleigh and love waves in the presence of low-velocity layers in near-surface seismic surveys: Surveys in Geophysics, **39**, 271–288, doi: 10.1007/s10712-017-9440-4.

Mi, B., J. Xia, C. Shen, L. Wang, Y. Hu, and F. Cheng, 2017, Horizontal resolution of multichannel analysis of surface waves: Geophysics, **82**, no. 3, EN51–EN66, doi: 10.1190/geo2016-0202.1.

Michaels, P., and P. E. J. McCabe, 1999,Interim URISP Report 10: Downhole seismic surveys SH- and P-waves: Technical Report, Boise State University Center for Geophysical Investigation of the Shallow Subsurface, 99–03.
Miller, R. D., J. Xia, C. B. Park, and J. Ivanov, 1999, Multichannel analysis of surface waves to map bedrock: The Leading Edge, **18**, 1392–1396, doi: 10.1190/1.1438226.
Molnar, S., J. F. Cassidy, S. Castellaro, C. Cornou, H. Crow, J. A. Hunter, S. Matsushima, F. J. Sánchez-Sesma, and A. Yong, 2018, Application of microtremor horizontal-to-vertical spectral ratio (MHVSR) analysis for site characterization: State of the art: Surveys in Geophysics, **39**, 613–631, doi: 10.1007/s10712-018-9464-4.
Nakamura, Y., 1989, A method for dynamic characteristics estimation of subsurface using microtremors on the ground surface: Quarterly Report of Railway Technical Research Institute, **30**, 25–33.
Okada, H., 2003, The microtremor survey method: SEG,Geophysical Monograph Series 12, 135.
Pan, Y., J. Xia, and C. Zeng, 2013, Verification of correctness of using real part of complex root as Rayleigh-wave phase velocity by synthetic data: Journal of Applied Geophysics, **88**, 94–100, doi: 10.1016/j.jappgeo.2012.09.012.
Park, C. B., R. D. Miller, and J. Xia, 1999, Multi-channel analysis of surface waves (MASW): Geophysics, **64**, 800–808, doi: 10.1190/1.1444590.
Picozzi, M., S. Parolai, and S. M. Richwalski, 2005, Joint inversion of H/V ratios and dispersion curves from seismic noise: Estimating the S-wave velocity of bedrock: Geophysical Research Letters, **32**, L11308, doi: 10.1029/2005GL022878.
Piña-Flores, J., M. Perton, A. García-Jerez, E. Carmona, F. Luzón, J. C. Molina-Villegas, and F. J. Sánchez-Sesma, 2017, The inversion of spectral ratio H/V in a layered system using the diffuse field assumption (DFA): Geophysical Journal International, **208**, 577–588, doi: 10.1093/gji/ggw416.
Sánchez-Sesma, F. J., M. Rodríguez, U. Iturrarán-Viveros, F. Luzón, M. Campillo, L. Margerin, A. García-Jerez, M. Suárez, M. A. Santoyo, and A. Rodríguez-Castellanos, 2011, A theory for microtremor H/V spectral ratio: Application for a layered medium: Geophysical Journal International, **186**, 221–225, doi: 10.1111/j.1365-246X.2011.05064.x.
Schwab, F. A., and L. Knopoff, 1972, Fast surface wave and free mode computations, *in* B. A. Bolt, ed., Methods in computational physics: Academic Press, 87–180.
Socco, L. V., S. Foti, and D. Boiero, 2010, Surface-wave analysis for building near-surface velocity models — Established approaches and new perspectives: Geophysics, **75**, no. 5, 75A83–75A102, doi: 10.1190/1.3479491.
Song, Y. Y., J. P. Castagna, R. A. Black, and R. W. Knapp, 1989, Sensitivity of near-surface shear-wave velocity determination from Rayleigh and love waves: 59th Annual International Meeting, SEG, Expanded Abstracts, 509–512, doi: 10.1190/1.1889669.
Thomson, W. T., 1950, Transmission of elastic waves through a stratified solid medium: Journal of Applied Physics, **21**, 89–93, doi: 10.1063/1.1699629.
Tuan, T. T., F. Scherbaum, and P. G. Malischewsky, 2011, On the relationship of peaks and troughs of ellipticity (H/V) of Rayleigh waves and the transmission response of single layer over half-space models: Geophysical Journal International, **184**, 793–800, doi: 10.1111/j.1365-246X.2010.04863.x.
Virieux, J., 1986, P-SV wave propagation in heterogeneous media: Velocity-stress finite-difference method: Geophysics, **51**, 889–901, doi: 10.1190/1.1442147.
Xia, J., 2014, Estimation of near-surface shear-wave velocities and quality factors using multichannel analysis of surface-wave methods: Journal of Applied Geophysics, **103**, 140–151, doi: 10.1016/j.jappgeo.2014.01.016.
Xia, J., R. D. Miller, and C. B. Park, 1999, Estimation of near-surface shear-wave velocity by inversion of Rayleigh wave: Geophysics, **64**, 691–700, doi: 10.1190/1.1444578.
Xu, Y., J. Xia, and R. D. Miller, 2007, Numerical investigation of implementation of air-earth boundary by acoustic-elastic boundary approach: Geophysics, **72**, no. 5, SM147–SM153, doi: 10.1190/1.2753831.
Zeng, C., J. Xia, R. D. Miller, and G. P. Tsoflias, 2011, Application of the multiaxial perfectly matched layer (M-PML) to near-surface seismic modeling with Rayleigh waves: Geophysics, **76**, no. 3, T43–T52, doi: 10.1190/1.3560019.